PROXIMITY-FED MIMO ANTENNA WITH TWO PRINTED IFAS AND A WIDEBAND T-SHAPED NEUTRALIZATION LINE

J.-F. Li[*] and Q.-X. Chu

School of Electronic and Information Engineering, South China University of Technology, Guangzhou 510640, China

Abstract—A proximity-fed MIMO (multiple-input-multiple-output) antenna with two printed IFAs (inverted-F antennas) and a wideband T-shaped neutralization line is presented. Each element printed IFA is fed by a proximity-fed structure which provides a parameter to control the return loss without effect on the isolation of the two IFAs. The wideband T-shaped neutralization line, which consists of two meandered branches and a rectangular grounded branch, can enhance the isolation of the two IFAs over a wide operation band (2.35–3.75 GHz). The two meandered branches are connected to the two IFAs, respectively, and the rectangular branch is connected to the ground plane. There are two parameters to adjust the isolation without effect on the return loss. Therefore, the operational bandwidth and the isolation of the proposed antenna can be controlled independently. A bandwidth of 46% with VSWR $\leq$ 2 and isolation $\geq$ 20 dB from 2.35 to 3.75 GHz is achieved. The MIMO antenna of compact size $40 \times 14 \, \text{mm}^2$ is suitable for application in mobile phones. Moreover, the ground plane size can be changed for applying the proposed antenna in different handsets. The results, including S-parameters, radiation pattern, mean effective gain (MEG), radiation efficiency, complex correlation coefficient and the effects of human hand and head, indicate the proposed MIMO antenna can provide spatial and pattern diversity.

* Corresponding author: Jian-Feng Li (li.jf01@mail.scut.edu.cn).

1. INTRODUCTION

The increasing demand for high quality and high data rate mobile communication calls for the development of MIMO systems [1]. However, it is very difficult to apply the MIMO scheme in small handsets such as mobile phones because the room for multiple antennas is extremely limited. The multiple antennas closely spaced will cause unwanted mutual coupling and low antenna efficiency, thus the performance of the MIMO system will be deteriorated. To reduce the mutual coupling, various methods had been developed by applying an inductor coil [2], orthogonal radiations [3], an inverted-Y shaped stub on the ground plane [4], and notches on the ground plane as resonators [5]. In [6], two different kinds of antenna are used to realize dual-band, but they were not operating in the same frequency band. Connecting (neutralization) lines were applied in [7–9], and the main advantage of this kind of isolation solution was its simplicity. However, the operation bands of the two PIFAs in [7] were different, and the connecting lines in [7–9] were only able to work within a narrow bandwidth. A study on the improvement of the neutralization line was presented in [10], and the design achieved the neutralization of the antennas through two meandered lines which were connected to the ground plane directly. Unfortunately, this way still only worked out within a narrow bandwidth.

In this paper, a coupled-fed MIMO antenna with two printed IFAs and a wideband T-shaped neutralization line is presented. Each element IFA is fed by a proximity-fed structure, which provides a parameter to control the return loss without effect on the isolation of the two IFAs. The wideband T-shaped neutralization line, which consists of two meandered branches and a rectangular grounded branch, can enhance the isolation of the two IFAs over a wide operation band (2.35–3.75 GHz). The two meandered branches are connected to the two IFAs, respectively, and the rectangular branch is connected to the ground plane. The wideband T-shaped neutralization line has two notable advantages over the conventional neutralization lines 1) it is able to work out across a wideband, and 2) the isolation can be controlled by two parameters without effect on the return loss. With the applications of the two proximity-fed structures and the T-shaped neutralization line, the operational bandwidth and the isolation can be controlled independently. The MIMO antenna of compact size $40 \times 14 \, \text{mm}^2$ is suitable for application in mobile phones. Moreover, the size of the ground plane can be changed for applying the antenna in different wireless handsets, and the variation of the ground plane size leads to no degradations of the operational bandwidth and isolation.
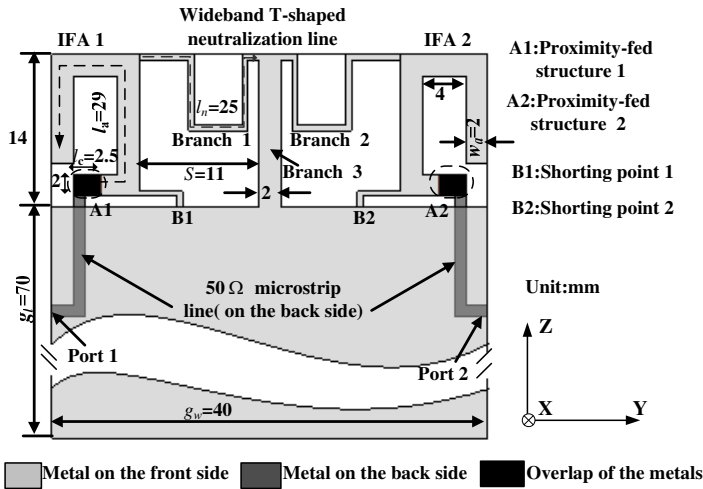
Figure 1. Geometry of the proposed MIMO antenna.

A bandwidth of 46% with VSWR ≤ 2 and isolation $\geq 20\,\text{dB}$ from 2.35 to 3.75 GHz is achieved, which covers 2.4-GHz WLAN and 2.5/3.5-GHz WiMAX. In Section 2, the geometry of the proposed MIMO antenna is presented. In Section 3, the operation mechanism of the MIMO antenna is investigated. To evaluate the diversity performance of the antenna, MEG, radiation efficiency and complex correlation coefficient of the antenna are calculated in Section 4. The effects of human hand and head on the radiation efficiency, total efficiency, total radiated power (TRP) and radiation pattern of the proposed antenna are discussed in Section 5 to provide quantifications for the performance of the MIMO antenna in real working conditions. Finally, a conclusion is given in Section 6. The simulated and the measured results are in a good agreement, thus the proposed MIMO antenna serving as a phone antenna can provide spatial and pattern diversity to increase data capacity of wireless communication systems.

2. GEOMETRY OF PROPOSED ANTENNA

The geometry of the proposed MIMO antenna is shown in Fig. 1. The two symmetric antenna elements (IFA 1 and 2) with length of $l_a = 29\,\text{mm}$ and width of $w_a = 2\,\text{mm}$ are positioned at the upper part of a partially grounded FR4 substrate with dimensions $84 \times 40 \times 0.8\,\text{mm}^3$, relative permittivity 4.4 and loss tangent 0.02. The two IFAs, ground plane of size $70\ (g_l) \times 40\,\text{mm}^2$ and a wideband T-shaped neutralization

line are printed on the front side of the FR4 substrate, while the two $50\,\Omega$ microstrip are printed on the back side of the substrate. The two proximity-fed structures with $2\,mm$ in width and $l_c = 2.5\,mm$ in length are the overlapping parts of the metal printed on the different sides of the substrate. The IFA 1 is fed by the proximity-fed structure 1and is grounded at shorting point 1. The IFA 2 is fed by the proximity-fed structure 2 and is grounded at shorting point 2. The wideband T-shaped neutralization line consists of two symmetric meandered branches (branch 1 and 2) and a rectangular grounded branch (branch 3). The branch 1 and 2 with $l_n = 25\,mm$ in length and $0.5\,mm$ in width are connected to the IFA 1 and 2, respectively, and the branch 3 of size $2 \times 14\,mm^2$ is connected to the ground plane.

3. DESIGN PROCESS AND OPERATION MECHANISM

All simulations are carried out using Ansoft HFSSv12, which is based on the finite element method (FEM) and the measurements are taken by Agilent N5230A vector network analyzer or in an anechoic chamber. The performance of the proposed MIMO antenna, especially the scattering parameters, will be analyzed in the following. $|S_{11}|$ denotes the reflection coefficient of the element IFA 1, and $|S_{21}|$ presents the mutual coupling between IFA 1 and IFA 2. Because of the symmetric configuration, $|S_{22}|$ is consistent with $|S_{11}|$, and $|S_{12}|$ is consistent with $|S_{21}|$. Therefore, only $|S_{11}|$ and $|S_{21}|$ are studied in this paper.

3.1. $\lambda/4$ Printed IFA

Investigations of the $\lambda/4$ printed single IFA as shown in Figs. 2 and 3 can help to understand the operation mechanism of the proposed printed MIMO antenna. In Figs. 2 and 3, the dimensions of the $\lambda/4$ IFAs, ground planes and FR4 substrates are the same as those given in Fig. 1. But this IFA is directly fed by introducing an via hole in Fig. 2, and l_c is selected to $2.8\,mm$ in Fig. 3.

In Fig. 2, the size of the IFA is $l_a \times w_a$, and the center operating frequency of the IFA can be approximately determined from [11]

$$f \approx \frac{c}{4(0.5l_a + w_a)} \times \frac{1}{\sqrt{(1 + \varepsilon_r)/2}} \tag{1}$$

where c and ε_r are the speed of light in free space and the relative permittivity of the substrate, respectively. Therefore, following (1) and finite-adjusting from experiments for the desired center frequency at $2.6\,GHz$, the dimensions of IFA are selected to $29 \times 2\,mm^2$ ($l_a \times w_a$). Fig. 2 shows the simulated $|S_{11}|$ as a function of l_a, it can be observed

that a $\lambda/4$ resonance excitation at about 2.6 GHz is produced when l_a is selected to 29 mm, but the operation band is poor.

Proximity-fed can help to enhance the operational bandwidth [12]. Therefore, the single IFA in Fig. 3 is fed by the proximity-fed structure with length l_c. Fig. 3 also shows the simulated $|S_{11}|$ with l_c varying from 2.3 to 3.3 mm while keeping the remaining dimensions fixed. It can be observed that a $\lambda/4$ dual-resonance excitation at about 2.6 GHz is produced, and the operation band is greatly improved as compared with Fig. 2. The increase of l_c corresponds to increase the capacitance of the input impedance, and the electrical length of the IFA is extended. Therefore, l_c is a parameter to adjust the operational bandwidth, and an operational band ranged from 2.15 to 3.81 GHz (VSWR $\leq$ 2) is achieved with $l_c = 2.8$ mm.

3.2. Study of the Mutual Coupling

The proximity-fed IFA discussed in the part 3.1 can be chosen as the element antenna of a MIMO antenna which is suitable for 2.4-GHz WLAN and 2.5/3.5-GHz WiMAX application. In Fig. 4, these two IFAs with edge-to-edge separation of $d = 24$ mm are integrated with a conventional ground plane. The dimensions of the IFAs, the ground plane and the FR4 substrate are fixed as shown in Fig. 3. Compared with the simulation result given in Fig. 3, this association of the two IFAs leads to better $|S_{11}|$ without any degradation of the operational bandwidth, but $|S_{21}|$ is only smaller than -9 dB over the whole band, and this indicates that the mutual coupling is strong.

One approach to explain the cause of the electromagnetic coupling between the IFAs located closely is to draw the intensity of the excited surface current distribution and analyze its magnitude level. The current distributions at the 2.3 and 3.2 GHz of the MIMO antenna
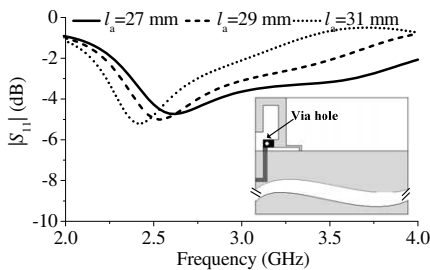

Figure 2. Structure of a directly-fed printed IFA and reflection coefficients of it with varying l_a.
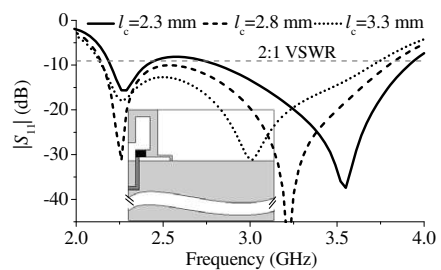
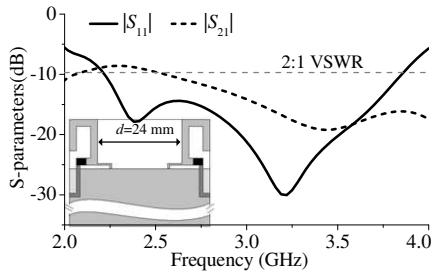**Figure 3.** Structure of a proximity-fed IFA and reflection coefficients of it with varying l_c.

Figure 4. Structure and S-parameters of a MIMO antenna with a conventional ground plane.
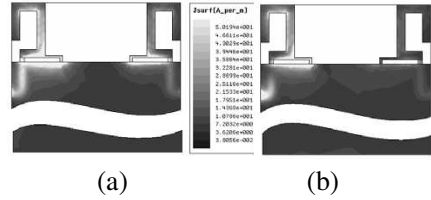
Figure 5. Current distributions of the antenna shown in Fig. 4 with IFA 1 excited and IFA 2 terminated with a $50\,\Omega$ load (a) at $2.3\,\text{GHz}$, (b) $3.2\,\text{GHz}$.
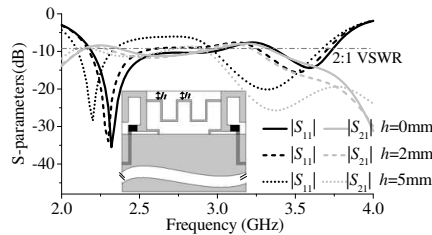

Figure 6. Structure of the MIMO antenna with a meandered neutralization line and S-parameters of the antenna with varying h.

with IFA 1 excited and IFA 2 terminated with a $50\,\Omega$ load are shown in Fig. 5. The excited IFA induces strong surface currents on the non-excited IFA, especially at $2.3\,\text{GHz}$, and that is the main reason of the poor isolation for the MIMO antenna.

3.3. Implementation of the Wideband T-shaped Neutralization Line

In Fig. 6, a meandered neutralization line is used. Two ends of the meandered line with length of $52\,\text{mm}$ (about 1λ at $3.4\,\text{GHz}$) and width of $0.5\,\text{mm}$ are connected to the two IFAs, respectively. If the meandered line is connected in a low impedance area of the IFAs, i.e., far away from its open end [7, 13], close to the vicinity of the feeding and the shorting strips where the currents have the highest intensity, it will not affect the frequency resonances and the operational bandwidth. However, this is not the case for the two proximity-fed printed IFAs.

The operational bandwidth is getting narrower and moves toward the low frequencies with the increase of h which means the meandered line is more closed to the two feeding ports and the two shorting points. When h is chosen as 5 mm, the curve of $|S_{21}|$ has one deep null (at about 3.2 GHz) and the mutual coupling for the upper part of the operational bandwidth is reduced greatly. However, the mutual coupling for the lower part of the operational bandwidth is still strong.

In order to get the low mutual coupling across the whole wideband of the MIMO antenna, a wideband T-shaped neutralization line described in Fig. 1 is applied. The proposed MIMO antenna has been fabricated and tested, and the photos of the fabricated MIMO antenna are shown in Fig. 7. In Fig. 8, it can be observed that the simulated and measured S-parameters are in a good agreement. An operational bandwidth of 46% with VSWR $\leq$ 2 and isolation $\geq$ 20 dB from 2.35 to 3.75 GHz covering the following bands: 2.4-GHz WLAN (2.4–2.484 GHz), 2.5-GHz WiMAX (2.5–2.69 GHz) and 3.5-GHz WiMAX (3.3–3.7 GHz), is achieved.

Due to the application of the wideband T-shaped neutralization line, 11 dB improvement of isolation across the whole bandwidth over the structures presented in Fig. 4 and Fig. 6 ($h = 5$ mm) are achieved. Only a small frequency shift-up for the operational bandwidth is observed in Fig. 8 as compared to the results in Fig. 3 ($l_c = 2.8$ mm) and Fig. 4. Fig. 9 shows the surface current distributions of the MIMO antenna at 2.4 and 3.4 GHz. When comparing with Fig. 5, the induced currents observed on the no excited IFA and its feeding port are weaker in Fig. 9. This helps to explain why the isolation is better for the design with the wideband T-shaped neutralization line.
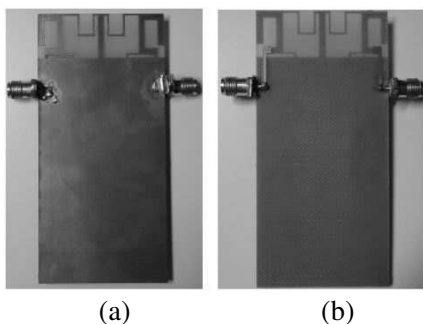

(a)   (b)

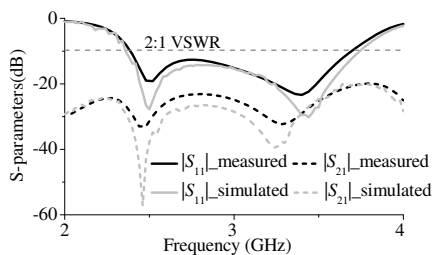**Figure 7.** Photographs of the fabricated antenna: (a) front view, (b) back view.

Figure 8. Simulated and measured S-parameters ofthe proposed MIMO antenna.
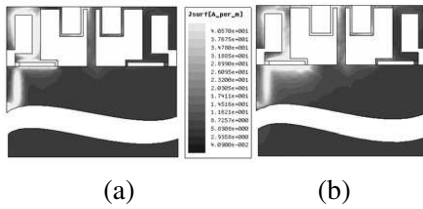
Figure 9. Current distributions of the proposedantenna with IFA 1 excited and IFA 2 terminated-with a 50 Ω load (a) at 2.4 GHz, (b) 3.4 GHz.
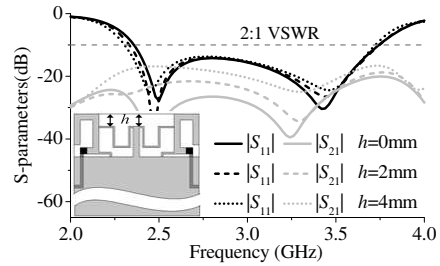

Figure 10. S-parameters of the proposed MIMO antenna with different h.

The goal of the conventional neutralization line [7–10] is to create an additional coupling path to compensate for the electrical currents flowing on the ground plane. Unfortunately, the technique is only suitable for the narrow band application because there is only one additional coupling path producing opposite coupling to the existing one to achieve a low mutual coupling at a chosen specific frequency. In this paper, the meandered branch 1 and 2 of the wideband T-shaped neutralization line are grounded to the ground plane and connected to each other by the rectangular branch 3. Thus, two additional coupling paths are realized. The coupling path 1 with length of 39 mm (about 0.5λ at 2.4 GHz), consists of one of the meandered branches and the rectangular branch 3. The coupling path 2 with length of 52 mm (about 1λ at 3.2 GHz), consists of the branch 1 and 2. The two additional coupling paths effectively compensate the original coupling of the antenna system. In Fig. 8, it can be seen that two deep nulls (at about 2.4 GHz and 3.2 GHz, respectively.) appear on the curve of $|S_{21}|$, and $|S_{21}|$ is better than -20 dB across the operational bandwidth. From Figs. 6 and 8, it can be concluded that the deep null at about 2.4 GHz is produced by the coupling path 1, and the deep null at about 3.2 GHz is produced by the coupling path 2.

The effect of the variation of h on the S-parameters is presented in Fig. 10, while keeping the remaining dimensions of the antenna geometry fixed as the geometry defined in Section 2. When h is increased, the length of the coupling path 1 is decreased, but the length of the coupling path 2 is fixed at 52 mm. Therefore, the variation of h has great effect on the deep null at about 2.4 GHz. This further illustrates that the deep null at about 2.4 GHz is produced by the

coupling path 1. In Fig. 6, it has been shown that the larger h leads to the operational bandwidth getting worse and moving toward the low frequencies. When the wideband T-shaped neutralization line is applied, the effect of the variation of h on the operational bandwidth can be neglected. However, the larger h produces poorer isolation, and that is contrary to the conclusions in [7–10]. The best result is achieved when h is selected to 0 mm. The length l_n of the meandered branches determines the lengths of both the two coupling paths, and therefore l_n has a great influence on the shape of the $|S_{21}|$ curve as shown in Fig. 11. Generally, the operational bandwidth is unchanged with varying h or l_n.

With the other parameters keeping fixed, the simulated S-parameters as a function of l_c is shown in Fig. 12. The operational bandwidth moves toward the lower frequencies with the increase of l_c, but the variation of l_c results in no shift of the two deep nulls observed on $|S_{21}|$ and no degradation of the magnitude of $|S_{21}|$. From Figs. 10, 11 and 12, it can be concluded that $|S_{11}|$ and $|S_{21}|$ of the proposed antenna can be controlled independently due to the application of the two proximity-fed structures and the T-shaped neutralization line.

In practice, the size of a wireless handset may be larger or smaller than the size of the proposed antenna. Therefore, the influence of the variations of the width g_w and the length g_l of the ground plane should be investigated. The effects of g_w and g_l on S-parameters are studied in Figs. 13 and 14, respectively, and l_c is fixed at 2.5 mm for the two cases. It is observed that the effects of g_w on $|S_{11}|$ and $|S_{21}|$ are slight. But the variation of g_l has great effect on the distribution of the surface ground current, and thus the mutual coupling is sensitive to the varying g_l. However, the mutual coupling is still better than -20 dB for all the cases as shown in Fig. 14. Therefore, the size of
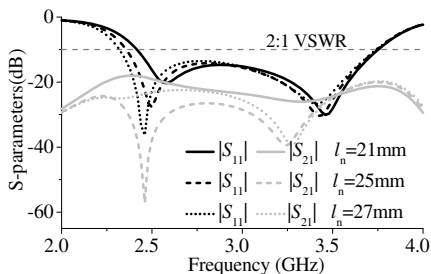

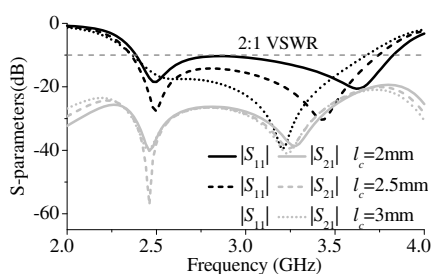**Figure 11.** S-parameters of the proposed MIMO antenna with different l_n.

Figure 12. S-parameters of the proposed MIMO antenna with different l_c.
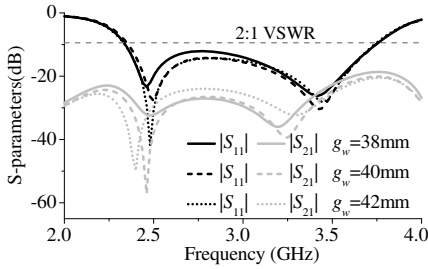
Figure 13. *S*-parameters of the proposed MIMOantenna with different g_w.
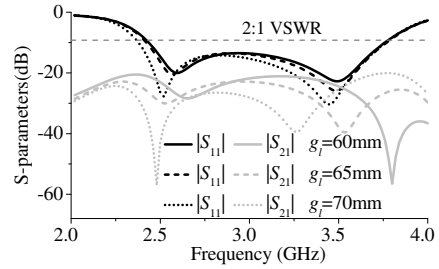
Figure 14. *S*-parameters of the proposed MIMO antenna with different g_l.

proposed antenna can be changed for applying in handsets of different sizes.

4. DIVERSITY PERFORMANCE OF THE PROPOSED MIMO ANTENNA

In the paper, the diversity performance of the MIMO antenna is evaluated by the radiation pattern, MEG, radiation efficiency η_{rad}, total efficiency η_{tot} and complex correlation coefficient ρ_c.

Figure 15 displays the simulated and measured 2-D radiation patterns of the two element IFAs (the tested IFA is excited, while the other one is terminated with a 50-Ω load) at 2.4 and 3.4 GHz, and the gains are normalized in here. It can be observed that the simulated and the measured results are in a good agreement. The gain patterns at 2.4 and 3.4 GHz are respectively plotted in Figs. 15(a) and (c) in the horizontal plane of the PCB and show almost omnidirectional character.

To quantify the average received signal strength for each IFA, MEGs are calculated based on a series of the assumption of mobile wireless environments defined in [14]. In this paper, a cross-polarization discrimination Γ of 0 dB, which is the average in an indoor fading environment [14], is assumed. MEGs at 2.4 and 3.4 GHz are calculated [15], and the calculated MEGs, ratios of MEG_i to MEG_j ($i, j = 1, 2$), η_{rad} and η_{tot}, which are obtained from the measured data, are listed in Table 1. The maximum ratio of MEG_i to MEG_j is smaller than 0.3 dB, and η_{rad} and η_{tot} are higher than 84% and 80%, respectively.

For isotropic/uniform signal propagation environments, the complex correlation coefficient ρ_c and envelope correlation coefficient
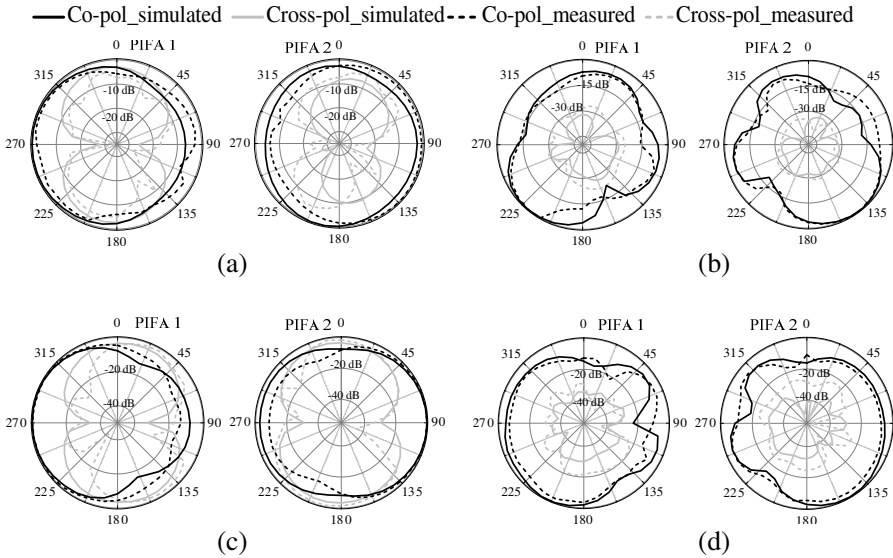
Figure 15. Simulated and measured radiation patterns at 2.4 GHz: (a) H-plane, (b) E-plane, at 3.4 GHz: (c).

ρ_e can be derived from the S-parameters [16], and they are denoted as ρ_c^s and ρ_e^s, respectively. Based on the conclusion in [17], ρ_c^s and ρ_e^s can be calculated by:

$$|\rho_{cij}^s|^2 = \rho_{eij}^s = \left| \frac{\left| S_{ii}^* S_{ij} + S_{ji}^* S_{jj} \right|}{\left| \left(1 - |S_{ii}|^2 - |S_{ji}|^2 \right) \left(1 - |S_{jj}|^2 - |S_{ij}|^2 \right) \eta_{radi} \eta_{radj} \right|^{1/2}} \right|^2 \tag{2}$$

The expression contains the effect of η_{rad} on ρ_c^s. For the Gaussian signal propagation environments: P_θ and P_φ are the θ and φ components of the probability distribution function of the incoming wave, respectively, $P_\theta(\theta)$ and $P_\varphi(\theta)$ being Gaussian distributed, and $P_\theta(\varphi)$ and $P_\varphi(\varphi)$ being uniform distributed. ρ_c and ρ_e can be evaluated from the radiation pattern [1] and are denoted as ρ_c^{rp} and ρ_e^{rp}, respectively:

$$|\rho_{ij}^{rp}|^2 = \rho_{eij}^{rp} = \left| \frac{\oint A_{ij}(\Omega) d\Omega}{\sqrt{\oint A_{ii}(\Omega) d\Omega \cdot \oint A_{ii}(\Omega) d\Omega}} \right|^2 \tag{3}$$

$$A_{ij}(\Omega) = \Gamma \cdot E_{\theta i}(\Omega) \cdot E_{\theta j}^*(\Omega) \cdot p_\theta(\Omega) + E_{\varphi i}(\Omega) \cdot E_{\varphi j}^*(\Omega) \cdot p_\varphi(\Omega) \tag{4}$$

where E_θ and E_φ are the θ and φ components of the complex electric field radiation pattern, respectively, and the asterisk presents the complex conjugate. Based on the measured data, the results are calculated and listed in Table 1 too. It can be observed that ρ_c is smaller than 0.1 for the two propagation environments.

5. EFFECT OF HAND AND HEAD

With the aid of simulation software SEMCAD-X [18], the effects of human hand and head on η_{rad}, TRP and radiation pattern of the proposed MIMO antenna are investigated. The input power in this paper is normalized to 1 W or 30 dBm [19].

The specific anthropomorphic mannequin (SAM) head [20] is used in this paper. The simulation model of the proposed MIMO antenna plus hand phantom is shown in Fig. 16(a). The simulation model of the MIMO antenna plus hand phantom and plus SAM head as shown in Fig. 16(b) represents the calling mode. Both for Figs. 16 (a) and 16(b), the MIMO antenna and the system ground plane are covered by a plastic casing with 1 mm in thickness to avoid the direct contact between the antenna and the hand/head model.

From Tables 1 and 2, it can be seen that η_{rad} and η_{tot} of the MIMO

Table 1. Performance of the proposed MIMO antenna.

f (GHz)	MEG$_1$ (dB)	MEG$_2$ (dB)	|MEG$_1$/MEG$_2$| (dB)	$(\eta_{rad})_1$ (%)	$(\eta_{rad})_2$ (%)	$(\eta_{tot})_1$ (%)	$(\eta_{tot})_2$ (%)	$\rho_{c12}^s \approx \rho_{c21}^s$	$\rho_{c12}^{rp} \approx \rho_{c21}^{rp}$
2.4	−3.98	−3.75	0.22	84.5	86.2	80.1	84.2	0.038	0.059
3.4	−3.61	−3.85	0.24	87.3	89.5	87.2	82.5	0.052	0.046

Table 2. Simulated effects of the hand and head on the proposed mimo antenna.

f (GHz)	MIMO antenna plus hand phantom						MIMO antenna plus hand phantom and plus SAM head					
	$(\eta_{rad})_1$ (%)	$(\eta_{tot})_1$ (%)	TRP$_1$ (dBm)	$(\eta_{rad})_2$ (%)	$(\eta_{tot})_2$ (%)	TRP$_2$ (dBm)	$(\eta_{rad})_1$ (%)	$(\eta_{tot})_1$ (%)	TRP$_1$ (dBm)	$(\eta_{rad})_2$ (%)	$(\eta_{tot})_2$ (%)	TRP$_2$ (dBm)
2.4	41.0	38.5	25.9	58.5	52.6	27.2	25.1	23.8	25.9	23.8	39.2	44.3
3.4	52.8	51.5	27.1	58.9	53.5	27.8	32.1	28.3	24.5	44.8	40.7	26.3

(a)   (b)

Figure 16. Configurations of (a) MIMO antenna plus hand phantom, (b) MIMO antenna plus hand phantomand plus SAM head.

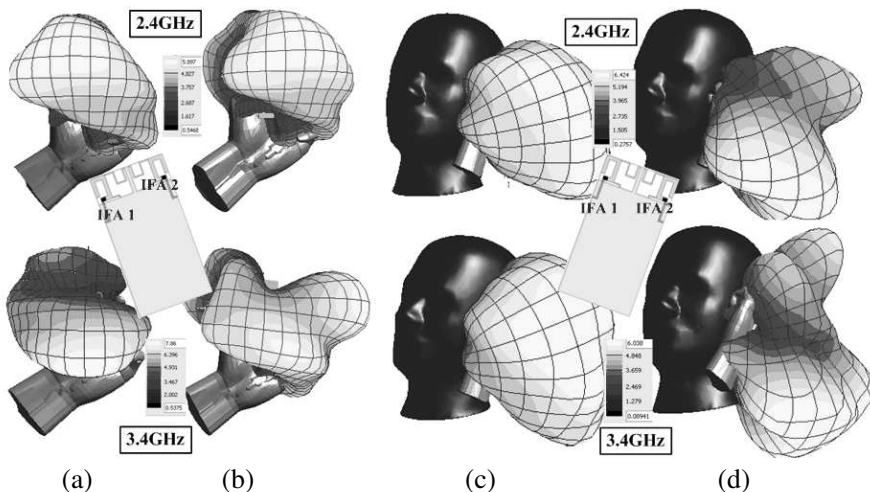(a)   (b)   (c)   (d)

Figure 17. Simulated 3-D radiation patterns for (a) MIMO antenna plushand phantom with IFA 1 excided and IFA 2 terminated with a 50-Ω load, (b) MIMO antenna plushand phantom with IFA 2 excided and IFA 1 terminated with a 50-Ω load, (c) MIMO antenna plus hand phantom and plusSAM head with IFA 1 excided and IFA 2 terminated with a 50-Ω load, (d) MIMO antenna plus hand phantom and plus SAM head with IFA 2 excided and IFA 1 terminated with a 50-Ω load.

antenna plus hand phantom are smaller than the MIMO antenna in free space because some power is absorbed by the hand phantom. The ground surface currents in Fig. 9 mainly concentrate on the upper part of the ground plane, and Figs. 13 and 14 show that the size variation of the ground plane has slight effect on the antenna performances. It may be concluded that the proposed antenna has strong robust or stable

performance. Therefore, η_{rad} and η_{tot} in Table 2, are sill larger than 38% and 41%, respectively. The SAM head also causes some power loss. Compared with the MIMO antenna plus hand phantom, η_{rad}, η_{tot} and TRPs of the MIMO antenna plus hand phantom and plus SAM head are smaller but still larger than 25%, 23% and 20 dBm, respectively. In Table 2, discrepancies of η_{rad}, η_{tot} and TRPs can be seen between the two IFAs because the relative positions of the hand and head for the two IFAs are different.

Figure 17 plots the simulated three-dimensional radiation patterns of the MIMO antenna plus hand phantom and MIMO antenna plus hand phantom and plus SAM head. The distortions of the radiation patterns due to the presence of the hand phantom/SAM head are small. Back-radiation patterns for the two IFAs are still achieved because of the robust or stable performance of the proposed antenna, and these special patterns are helpful for receiving or transmitting signal in all directions and reduce the mutual coupling caused by the near-field. All the results show that the proposed MIMO antenna has good pattern diversity in real-world usage conditions.

6. CONCLUSION

The proximity-fed MIMO antenna with two printed IFAs and a wideband T-shaped neutralization line has been studied. A operational bandwidth of 46% with $|S_{11}| \leq -10$ dB and $|S_{21}| \leq -20$ dB from 2.35 to 3.75 GHz covering the follow bands: 2.4-GHz WLAN and 2.5/3.5-GHz WiMAX, has been achieved. Each element IFA is fed by a proximity-fed structure which provides a parameter to tune the return loss without effect on the isolation. The wideband T-shaped neutralization line has been introduced, which can reduce the mutual coupling across the whole wide operational bandwidth. Moreover, there are two parameters to control the isolation without effect on the return loss. Therefore, the return loss and the isolation can be controlled independently. The size of the ground plane can be changed for applying the proposed MIMO antenna in wireless handsets of different sizes. MEG, radiation/total efficiencies and correlation coefficient have been calculated, and the effects of human hand and head have also been studied. All the results shows that the wideband T-shaped neutralization line is a simple and effective way to reduce the mutual coupling and the proposed antenna serving as a phone MIMO antenna can provide spatial and pattern diversity to increase data capacity of wireless communication systems in real-world usage conditions.

ACKNOWLEDGMENT

REFERENCES

1. Vaughan, R. G. and J. B. Anderson, "Antenna diversity in mobile communications," *IEEE Trans. Veh. Technol.*, Vol. 36, No. 4, 147–172, Nov. 1987.

2. Krairiksh, M., P. Keowsawat, C. Phongcharoenpanich, and S. Kosulvit, "Two-probe excited circular ring antenna for MIMO application," *Progress In Electromagnetics Research*, Vol. 97, 417–431, 2009.

3. Bae, S., Y.-K. Hong, J.-J. Lee, J.-H. Park, J. Jalli, G. Abo, H. M. Kwon, and C. K. K. Jayasooriya, "Miniature and higher-order mode ferrite MIMO ring patch antenna for mobile communication system," *Progress In Electromagnetics Research B*, Vol. 25, 53–74, 2010.

4. Najam, A. I., Y. Duroc, and S. Tedjni, "UWB-MIMO antenna with novel stub structure," *Progress In Electromagnetics Research C*, Vol. 19, 245–257, 2011.

5. Kim, K. J. and K. H. Ahn, "The high isolation dual-band inverted F antenna diversity system with the small N-section resonators on the ground plane," *Microw. Opt. Technol. Letter*, Vol. 49, No. 3, 731–734, Mar. 2007.

6. Min, K. S., M.-S. Kim, C.-K. Park, and M. D. Vu, "Design for PCS antenna based on WiBro-MIMO," *Progress In Electromagnetics Research Letters*, Vol. 1, 77–83, 2008.

7. Diallo, A., C. Luxey, and P. L. Thuc, "Study and reduction of the mutual coupling between two mobile phone IFAs operating in the DCS 1800 and UMTS bands," *IEEE Trans. Antennas Propag.*, Vol. 54, No. 11, 3063–3074, 2006.

8. Mak, A. C. K., C. R. Rowell, and R. D. Murch, "Isolation enhancement between two closely packed antennas," *IEEE Trans. Antennas Propag.*, Vol. 56, No. 11, 3411–3419, 2008.

9. Yang, C., J. Kim, and H. Kim, "Quad-band antenna with high isolation MIMO and broadband SCS for broadcasting and telecommunication services," *IEEE Antennas and Wireless Propag. Letter*, Vol. 9, 584–587, 2010.

10. Chebihi, A., L. Cyril, and S. Robert, "A novel isolation technique

for closely spaced PIFAs for UMTS mobile phones," *IEEE Antennas and Wireless Propag. Letter*, Vol. 7, 665–668, 2008.

11. Wong, K. L., S. W. Su, and C. L. Tang, "Internal shorted patch antenna for a UMTS folder-type mobile phone," *IEEE Trans. Antennas Propag.*, Vol. 53, No. 10, 3391–3394, 2005.

12. Chang, C. H. and K. L. Wong, "Internal coupled-fed shorted monopole Antenna for GSM850/900/1800/1900/UMTS operation in the laptop computer," *IEEE Trans. Antennas Propag.*, Vol. 56, No. 11, 3600–3604, Nov. 2008.

13. Carrasco, H., H. D. Hristov, R. Feick, and D. Cofré, "Mutual coupling between planar inverted-F antennas," *Microwave Opt. Technol. Letter,* Vol. 42, No. 3, 224–227, Aug. 15, 2004.

14. Sammuel, C. S. K. and R. D. Murch, "Compact integrated diversity antenna for wireless communications," *IEEE Trans. Antennas Propag.*, Vol. 49, No. 6, 954–960, Jun. 2001.

15. Karaboikis, M., C. Soras, G. Tsachtsiris, and V. Makios, "Compact dual-printed inverted-F antenna diversity systems for portable wireless devices," *IEEE Trans. Antennas and Wireless Propag. Letter*, Vol. 3, 9–14, 2004.

16. Blanch, S., J. Romeu, and I. Corbella, "Exact representation of antenna system diversity performance from input parameter description," *IEE Electron. Letter*, Vol. 39, No. 9, 705–707, May 1, 2003.

17. Hallbjorner, P., "The significance of radiation efficiencies when using S-parameterss to calculate the received signal correlation from two antennas," *IEEE Antennas and Wireless Propag. Letter*, Vol. 4, 97–99, 2005.

18. Available at: http://www.semcad.com, SPEAG SEMCAD, Schmid and Partner Engineering AG.

19. Li, C. H., E. Ofli, N. Chavannes, and N. Kuste, "Effects of hand phantom on mobile phone antenna performance," *IEEE Trans. Antennas Propag.*, Vol. 57, No. 9, 2763–2770, Sep. 2009.

20. IEEE recommended practice for determining the peak spatial-average specific absorption rate (SAR) in the human head from wireless communications devices: Measurement techniques, IEEE Standard 1528, IEEE Standards Coordinating Committee 34, Dec. 2003.